Discovering heavy neutrino oscillations in rare $B_c^{\pm}$ meson decays at HL-LHCb

Sebastian Tapia,[1,*] Marcelo Vidal-Bravo,[2,3,†] and Jilberto Zamora-Saá[2,3,‡]

[1]Department of Physics and Astronomy, Iowa State University, Ames, Iowa 50010, USA
[2]Center for Theoretical and Experimental Particle Physics, Facultad de Ciencias Exactas, Universidad Andres Bello, Fernandez Concha 700, Santiago, Chile
[3]Millennium Institute for Subatomic physics at high energy frontier-SAPHIR, Fernandez Concha 700, Santiago, Chile

(Received 20 September 2021; accepted 17 January 2022; published 2 February 2022)

In this work, we study the lepton flavor and lepton number violating B_c meson decays via two intermediate on-shell Majorana neutrinos N_j into two charged leptons and a charged pion $B_c^{\pm} \to \mu^{\pm} N_j \to \mu^{\pm}\tau^{\pm}\pi^{\mp}$. We evaluated the possibility to measure the modulation of the decay width along the detector length produced as a consequence of the lepton flavor violating process, in a scenario where the heavy neutrinos masses range between 2.0 GeV $\leq M_N \leq$ 6.0 GeV. We study some realistic conditions, which could lead to the observation of this phenomenon at future B factories, such as the HL-LHCb.

DOI: 10.1103/PhysRevD.105.035003

I. INTRODUCTION

The first indications of physics beyond the standard model (SM) come from the baryonic asymmetry of the universe (BAU), dark matter (DM), and neutrino oscillations (NOs). In last decades NOs experiments have shown that active neutrinos (ν) are very light massive particles $M_\nu \sim 1$ eV [1,2] and, consequently, the SM is not a final theory and must be extended. There are several SM extensions that allow explaining the small active neutrino masses, however, in this paper we pay attention to those based on the see-saw mechanism (SSM) [3,4]. The SSM introduces a new heavy Majorana particle (singlet under $SU(2)_L$ symmetry group), commonly called heavy neutrino (HN), which by means of inducing a dimension-five operator [5] leads to a very light active Majorana neutrino. These newly introduced HNs have a highly suppressed interaction with gauge bosons (Z, $W^{\pm}$) and leptons (e, μ, τ), making its detection a challenging task. However, although this suppression, the existence of HNs can be explored via rare meson decays [6–20], colliders [21–39], and tau factories [40–43].

One of the most promising SM extensions based on the SSM is the neutrino-minimal standard model (νMSM) [44,45], which introduces two almost degenerate HNs with masses $M_{N1} \approx M_{N2} \sim 1$ GeV, and a third HN with mass $M_{N3} \sim$ keV, which is a natural candidate for DM. Apart to explain the small active neutrino masses, the νMSM allows to explain successfully the BAU by means of "leptogenesis from HNs oscillations," also known as the Akhmedov-Rubakov-Smirnov mechanism [46].

In a previous article [15], we have described the effects of heavy neutrino oscillations (HNOs) in the so-called rare lepton number violating (LNV) and lepton flavor violating (LFV) pseudoscalar B meson decays, via two almost degenerate heavy on-shell Majorana neutrinos ($M_{N_i} \sim 1$ GeV), which can oscillate among themselves. The aim of this article is to develop a more realistic analysis of the experimental conditions needed to detect the aforementioned phenomenon. We will focus especially on the high luminosity LHCb (HL-LHCb), which due to its excellent detector resolution [47,48] could make possible the observation of the HNOs. Similar studies have been performed for other experiments (see Refs. [20,34,41,49]).

The work is arranged as follows: In Sec. II, we study the production of the heavy neutrinos in $B_c^{\pm}$ meson decays. In Sec. III, we describe the simulations of the HN production. In Sec. IV, we present the results and a discussion of it, and in Sec. V we provide a brief summary of the article.

II. PRODUCTION OF THE RIGHT-HANDED NEUTRINOS

As we stated above, we are interested in studying the lepton flavor and lepton number violation processes

*s.tapia@cern.ch
†M.vidalbravo@uandresbello.edu
‡jilberto.zamora@unab.cl; jilberto.zamorasaa@cern.ch

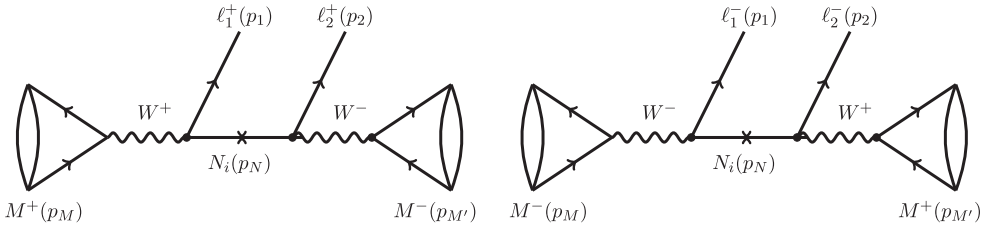

FIG. 1. The $M^{\pm}$ pseudoscalar meson decays, intermediated by heavy neutrinos. Left panel: Feynman diagrams for the LFV and LNV process $M^+ \to \ell_1^+ \ell_2^+ \pi^-$. Right panel: Feynman diagrams for the LFV and LNV process $B^- \to \ell_1^- \ell_2^- \pi^+$. We remark that in this study, we will consider $M = B_c$, $M' = \pi$, $\ell_1 = \mu$ and $\ell_2 = \tau$.

$(B_c^{\pm} \to \mu^{\pm} N_j \to \mu^{\pm} \tau^{\pm} \pi^{\mp})$, which are characterized by the following Feynman diagrams (Fig. 1). In this work we will consider the scenario where the two heavy neutrino (N_1 and N_2) masses fall in the range of a few GeVs and are almost degenerate ($M_{N_1} \approx M_{N_2}$). The mixing coefficient between the standard flavor neutrino ν_ℓ ($\ell = e, \mu, \tau$) and the heavy mass eigenstate N_i is $B_{\ell N_i}$ (i = 1, 2), then the light neutrino flavor state can be defined as

$$\nu_\ell = \sum_{i=1}^{3} B_{\ell \nu_i} \nu_i + \underbrace{(B_{\ell N_1} N_1 + B_{\ell N_2} N_2)}_{\text{Heavy Neutrino Sector}}, \tag{1}$$

where $B_{\ell \nu_i}$ (i = 1, 2, 3), and $B_{\ell N_j}$ (j = 1, 2) are the complex elements of the 5×5 Pontecorvo–Maki–Nakagawa–Sakata (PMNS) matrix, and will be parametrized as follows:

$$\begin{aligned} B_{\ell \nu_i} &= |B_{\ell \nu_i}| e^{i\theta_{\ell i}}, \qquad (i = 1, 2, 3) \quad \text{and} \\ B_{\ell N_j} &= |B_{\ell N_j}| e^{i\theta_{\ell N_j}}, \qquad (j = 1, 2). \end{aligned} \tag{2}$$

The mass difference between HNs is expressed as ($|\Delta M_N| = M_{N2} - M_{N1} \equiv Y \Gamma_N$), where Y stands to measures the mass difference in terms of $\Gamma_N = (1/2)(\Gamma_{N_1} + \Gamma_{N_2})$, which is the

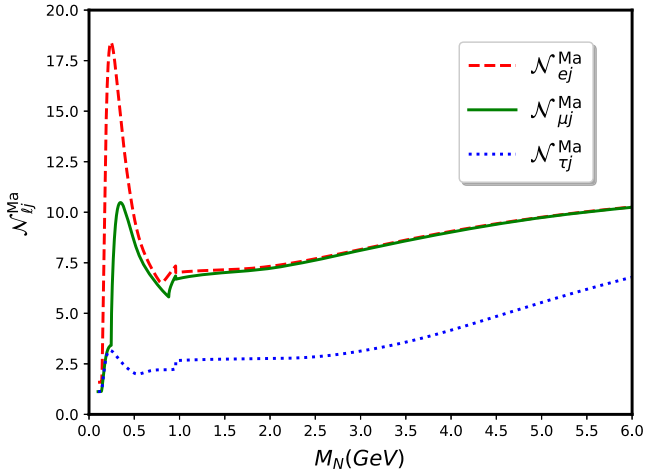

FIG. 2. Effective mixing coefficients $\mathcal{N}_{\ell j}^{\mathrm{Ma}}$ for Majorana neutrinos. Data taken from [50].

(average of the) total decay width of the intermediate heavy neutrino. The decay width $\Gamma_{\mathrm{Ma}}(M_{N_i})$ of a single heavy neutrino N_i is

$$\Gamma_{\mathrm{Ma}}(M_{N_i}) \equiv \Gamma_{N_i} \approx \mathcal{K}_i^{\mathrm{Ma}} \frac{G_F^2 M_{N_i}^5}{96\pi^3}, \tag{3}$$

where

$$\mathcal{K}_i^{\mathrm{Ma}} = \mathcal{N}_{ei}^{\mathrm{Ma}} |B_{eN_i}|^2 + \mathcal{N}_{\mu i}^{\mathrm{Ma}} |B_{\mu N_i}|^2 + \mathcal{N}_{\tau i}^{\mathrm{Ma}} |B_{\tau N_i}|^2. \tag{4}$$

Here the factors $B_{\ell N}$ are the heavy-light mixing elements of the PMNS matrix[1] and $\mathcal{N}_{\ell i}^{\mathrm{Ma}}$ are the effective mixing coefficients, which account for all possible decay channels of N_i and are presented in Fig. 2 for our M_N range of interest ($0 \le M_N \le 6$ GeV).

It is important to mention that, due to the dependency on $|B_{\ell N_i}|$, the factors $\mathcal{K}_i^{\mathrm{Ma}}$ could be, in principle, different for N_1 and N_2, that means it is possible that $|B_{\ell N_1}| \neq |B_{\ell N_2}$ and, consequently, $\mathcal{K}_1^{\mathrm{Ma}}$ dominate over $\mathcal{K}_2^{\mathrm{Ma}}$ or vice versa. The factors $\mathcal{K}_i^{\mathrm{Ma}}$ only appear in $\Gamma_N(M_{N_i})$ (Eq. (3), all our numerical calculations have been performed for $\Gamma_N = (1/2)(\Gamma_{N_1} + \Gamma_{N_2})$, i.e., $\Gamma_N(M_N) \approx \Gamma_N(M_{N_1})/2$ if $\mathcal{K}_1^{\mathrm{Ma}} \gg \mathcal{K}_2^{\mathrm{Ma}}$ and $\Gamma_N(M_N) \approx \Gamma_N(M_{N_2})/2$ if $\mathcal{K}_2^{\mathrm{Ma}} \gg \mathcal{K}_1^{\mathrm{Ma}}$, then it is not expected to have a significant impact if one factor dominates over the other. However, in this work we will assume that $\mathcal{K}_1^{\mathrm{Ma}} \approx \mathcal{K}_2^{\mathrm{Ma}} \equiv \mathcal{K}$. In addition, we will consider the mixing elements $|B_{\mu N_i}|^2 \approx |B_{\tau N_i}|^2 \equiv |B_{\ell N_i}|^2 = 10^{-5}$, $\mathcal{N}_{ei}^{\mathrm{Ma}} |B_{eN_i}|^2 \approx 0$ and $\mathcal{N}_{\mu i}^{\mathrm{Ma}} + \mathcal{N}_{\tau i}^{\mathrm{Ma}} \approx 15$; hence, $\mathcal{K}^{\mathrm{Ma}} = 15 |B_{\ell N}|^2$. As a consequence of the aforementioned, the HN total decay width are almost equals ($\Gamma_{N_1} \approx \Gamma_{N_2}$) and can be written as

$$\Gamma_{\mathrm{Ma}}(M_{N_i}) \equiv \Gamma_N(M_N) = 15 |B_{\ell N}|^2 \frac{G_F^2 M_N^5}{96\pi^3}. \tag{5}$$

[1]In this work we define the light neutrino flavor state as $\nu_\ell = \sum_{i=1}^{3} U_{\ell i} \nu_i + \sum_{j=1}^{2} B_{\ell N} N_j$. However, other authors also use $U_{\ell N}$ or $V_{\ell N}$ as the heavy-light mixing elements (i.e., $B_{\ell N} \equiv U_{\ell N} \equiv V_{\ell N}$).

In Ref. [15] it was obtained that the L-dependent effective differential decay width, considering the effect of HNOs [see Eq. (6)] and considering the effects of a detector of length L, for fixed values[2] of HN velocity ($\equiv\beta_N$) and the HN Lorentz factor ($\equiv\gamma_N$) is

$$\frac{d}{dL}\Gamma(M^{\pm}) = \frac{e^{\frac{-L\Gamma_N}{\gamma_N\beta_N}}}{\gamma_N\beta_N}\tilde{\Gamma}(M^{+}\to \ell_1^{+}N)\tilde{\Gamma}(N\to \ell_2^{+}M'^{-}) \times\left(\sum_{i=1}^{2}|B_{\ell_1 N_i}|^2|B_{\ell_2 N_i}|^2 + 2|B_{\ell_1 N_1}||B_{\ell_2 N_1}||B_{\ell_1 N_2}||B_{\ell_2 N_2}|\cos\left(2\pi\frac{L}{L_{\rm osc}}\pm\theta_{LV}\right)\right), \tag{6}$$

where $L_{\rm osc} = (2\pi\beta_N\gamma_N)/\Delta M_N$ is the HN oscillation length, and the angle θ_{LV} stands for the relative CP-violating phase between N_1 and N_2 that comes from the $B_{\ell N_i}$ elements[3] and is given by

$$\theta_{LV} = \arg(B_{\mu N_2}) + \arg(B_{\tau N_2}) - \arg(B_{\mu N_1}) - \arg(B_{\tau N_1}). \tag{7}$$

It is worth it to mention that, in general, M is moving in the lab frame when it decays into N and ℓ_1, therefore, the product $\gamma_N\beta_N$ is not always fixed and can be written as

$$\beta_N\gamma_N = \sqrt{(E_N(\hat{p}'_N)/M_N)^2 - 1}, \tag{8}$$

where E_N is the heavy neutrino energy in the lab frame, depending on $\hat{p}'_N$ direction in the M-rest frame (Σ').

The relation among E_N, $\vec{p}'_N$ and the angle θ_N is given by the Lorentz energy transformation (see Fig. 3),

$$E_N = \gamma_M(E'_N + \cos\theta_N\beta_M|\vec{p}'_N|), \tag{9}$$

where the corresponding factors in the M-rest frame (Σ') are given by

$$E'_N = \frac{M_M^2 + M_N^2 - M_{\ell_1}^2}{2M_M}, \qquad |\vec{p}'_N| = \frac{1}{2}M_M\lambda^{1/2}\left(1, \frac{M_{\ell_1}^2}{M_M^2}, \frac{M_N^2}{M_M^2}\right). \tag{10}$$

We remark that β_M is the velocity of M in the lab frame, and $\lambda(x,y,z)$ is

$$\lambda(x,y,z) = x^2 + y^2 + z^2 - 2xy - 2xz - 2yz. \tag{11}$$

Therefore, Eq. (6) must be rewritten in differential form and integrated over all directions of heavy neutrino $\vec{p}'_N$ in the M-rest frame, in addition, we set $M\to B_c$, $\ell_1\to\mu$, $\ell_2\to\tau$ and $M'\to\pi$,

$$\frac{d}{dL}\Gamma^{\rm osc}_{LV}(B_c^{\pm}) = \int\frac{e^{\frac{-L\Gamma_N}{((E_N(\hat{p}'_N)/M_N)^2-1)^{1/2}}}}{((E_N(\hat{p}'_N)/M_N)^2-1)^{1/2}}d\Omega_{\hat{p}'_N}\frac{d\tilde{\Gamma}(B_c^{+}\to\mu^{+}N)}{d\Omega_{\hat{p}'_N}}\tilde{\Gamma}(N\to\tau^{+}\pi^{-}) \times\left(\sum_{i=1}^{2}|B_{\mu N_i}|^2|B_{\tau N_i}|^2 + 2|B_{\mu N_1}||B_{\tau N_1}||B_{\mu N_2}||B_{\tau N_2}|\cos\left(2\pi\frac{L}{L_{\rm osc}(\hat{p}'_N)}\pm\theta_{LV}\right)\right), \tag{12}$$

where $L_{\rm osc}(\hat{p}'_N)$ adopts the following form:

$$L_{\rm osc}(\hat{p}'_N) = \frac{2\pi\beta_N\gamma_N}{M_N} = \frac{2\pi}{M_N^2}|\vec{p}_N(\hat{p}'_N)| = \frac{2\pi}{M_N}[(E_N(\hat{p}'_N)/M_N)^2 - 1]^{1/2}, \tag{13}$$

and

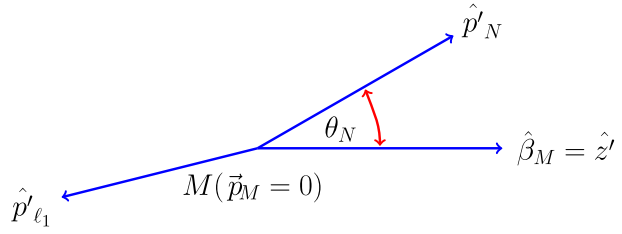

FIG. 3. The 3-momenta directions of leptons in the M-rest frame (Σ'). Here θ_N defines the angle between $\hat{\beta}_M$ and $\hat{p}'_N$, where $\hat{\beta}_M = \frac{\vec{\beta}_M}{|\vec{\beta}_M|}$ is the direction of the velocity of M in the lab frame; we notice that $\hat{\beta}_M$ also defines the $\hat{z}'$ axis.

[2]We notice that in the literature [13–15], in the laboratory frame (Σ), usually $\gamma_N\beta_N = 2$.

[3]It is important to note that if $\theta_{LV} = 0$, then there is no difference between $\frac{d}{dL}\Gamma(B^{+})$ and $\frac{d}{dL}\Gamma(B^{-})$.

$$\bar{\Gamma}(N \to \pi^{\pm}\tau^{\mp}) = \frac{1}{16\pi} G_F^2 f_\pi^2 |V_{ud}|^2 \frac{1}{M_N} \lambda^{1/2}\left(1, \frac{M_\pi^2}{M_N^2}, \frac{M_\tau^2}{M_N^2}\right) \times [(M_N^2 + M_\tau^2)(M_N^2 - M_\pi^2 + M_\tau^2) - 4M_N^2 M_\tau^2]. \quad (14)$$

The term $d\tilde{\Gamma}(B^+ \to \ell_1^+ N)/d\Omega_{\hat{p}'_N}$ is given by

$$\frac{d\tilde{\Gamma}(B_c^+ \to \mu^+ N)}{d\Omega_{\hat{p}'_N}} = \frac{1}{4\pi}\tilde{\Gamma}(B_c^+ \to \mu^+ N) \quad (15a)$$

$$= \frac{1}{32\pi^2} G_F^2 f_{B_c}^2 |V_{cb}|^2 M_{B_c}^3 \lambda^{1/2}(1, x_N, x_\mu)((1 - x_N)x_N + x_\mu(1 + 2x_N - x_\mu)) \quad (15b)$$

where $x_N = M_N^2/M_{B_c}^2$ and $x_\mu = M_\mu^2/M_{B_c}^2$. The Fermi constant is $G_F = 1.166 \times 10^{-5}$ GeV^{-2}, the meson decays constants are $f_\pi = 0.1304$ GeV and $f_{B_c} = 0.4$ GeV, the Cabibbo-Kobayashi-Maskawa elements are $|V_{ud}| = 0.974$ and $|V_{cb}| = 0.041$, and the masses are $M_{B_c} = 6.275$ GeV, $M_\pi = 139.57 \times 10^{-3}$ GeV, $M_\mu = 105.7 \times 10^{-3}$ GeV, and $M_\tau = 1.777$ GeV. It is worth mentioning that in Eq. (15) it has been performed, the average over B_c initial polarization and the sum over the helicities of μ^+ and N. Therefore, Eq. (12) is then only θ_N dependent [see Eqs. (9) and (10)], hence, the integration $d\Omega_{\hat{p}'_N}$ reduces to $2\pi d(\cos\theta_N)$.

III. HEAVY NEUTRINO PRODUCTION SIMULATIONS

For the correct evaluation of the quantities in Eq. (12), and to test the feasibility to measure the phenomenon described here, we require a realistic distribution of γ_M, which can lead to a realistic distribution of β_M through $\beta_M = \sqrt{1 - 1/\gamma_M^2}$. This realistic distribution is obtained by means of simulations of B_c mesons production via the charged current Drell-Yan process, using MADGRAPH5_aMC@NLO [51], PYTHIA8 [52], and Delphes [53] for B_c^+ and B_c^- individually (see Fig. 4) for LHCb conditions with $\sqrt{s} = 13$ TeV.

The observation of the studied phenomenon [Eq. (12)] depends on the number of produced B_c mesons (N_{B_c}) at the particular experiment. The HL-LCHb is designed to reach a luminosity $\mathcal{L} = 2 \times 10^{-34}$ cm^{-2} s^{-1} [54], transforming it into one of the most promising B factories. The B mesons production cross section is $\sigma_B \approx 86.6$ μb [55], however, σ_{B_c} is suppressed by a factor of 10^{-3} with respect to σ_B [56]; this suppression factor implies that for each 10^6 B mesons we have 10^3 B_c mesons. The HNs production has been calculated in detail in Refs. [12–14], in addition, assuming a 50% detector efficiency, the expected number of heavy neutrino events (with HNs masses between 3.5–5.5 GeV and $|B_{\ell N}|^2 = 10^{-5}$) can reach ≈3000 for six years of operation.

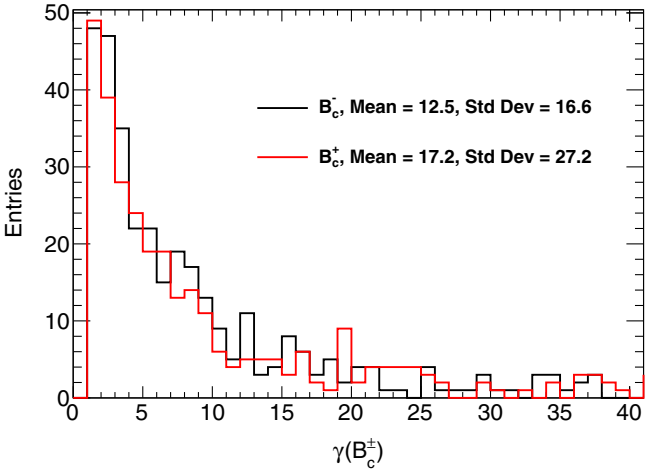

FIG. 4. The Lorentz $\gamma_{B_c^\pm}$ factor for $B_c^\pm$ mesons.

IV. RESULTS AND DISCUSSION

In this article, we have studied the modulation $d\Gamma(B_c)/dL$ for the LNV $B_c^\pm$ meson decays, assuming conditions that could be present at the LHCb experiment. We focus on a scenario that contains two almost degenerate (on-shell) heavy Majorana neutrinos. This scenario has been studied in previous work, Ref. [15], in which we have explored the modulation in a more academic frame. In this paper we consider more realistic conditions that could lead to a discovery in the upcoming years. Figure 5 shows the differential decay width $d\Gamma(B_c^\pm)/dL$ for fixed values of γ_N and β_N, which are determined from the average values of $\gamma_{B_c^\mp}$ presented in Fig. 4 for two values of θ_{LV}. The solid lines stand for the processes, which include the effects of HNOs, while the dashed lines do not. It could be seen that the effects of HNOs over $d\Gamma(B_c^\pm)/dL$ could enhance or decrease it near a factor of 2, in comparison with the case with NO-HNOs for some regions of L. In addition, for $d\Gamma(B_c^\pm)/dL$ with NO-HNOs effects, there is no modulation, and only exist the damping effect produced due to the probability that the HN decay.

We noticed that the difference between the process for B_c^+ and B_c^- is maximized when the CP-violation angle is $\theta_{LV} = \pi/2$ [as expected from Eq. (12)]. We also observed that as the distance L grows, both curves tend to converge; this is because as the HN propagates, the cumulative probability that the HN has decayed is greater. This effect is characterized by the exponential factor present in $d\Gamma(B_c)/dL$ [Eq. (12)], which specifically accounts for the probability that the HN decays within the detector of length L.

Figures 6 and 7 show the differential decay width $d\Gamma(B_c)/dL$ for nonfixed values (nonaverage values) of γ_N and β_N, which are determined from the simulated distributions of $\gamma_{B_c^\pm}$ presented in Fig. 4. Figures 6 and 7 were performed for $\theta_{LV} = \pi/2$ and $\theta_{LV} = \pi/4$, respectively, and two values of M_N. The effects of nonfixed γ_N

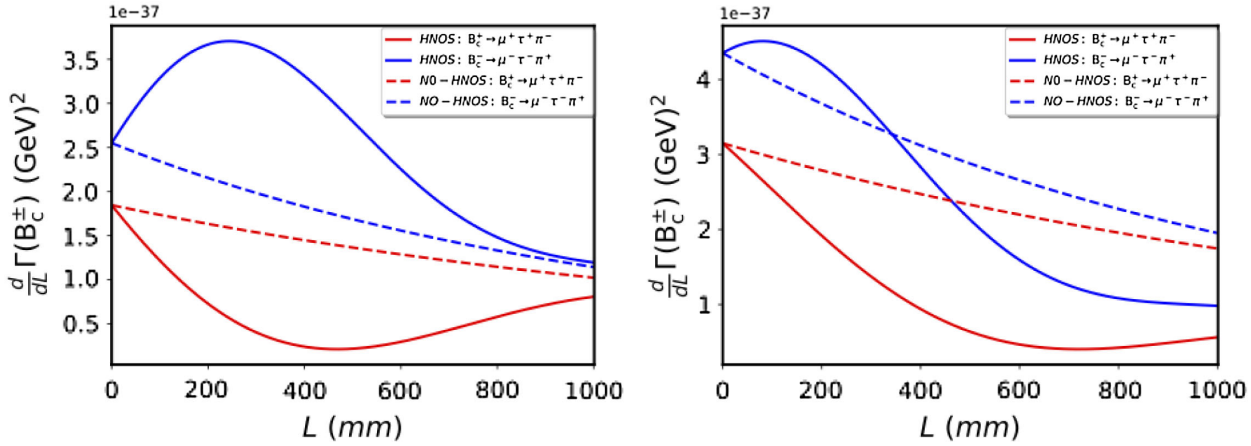

FIG. 5. Differential decay width $d\Gamma(B_c)/dL$ for average value of $\gamma_{B_c^\pm}$. Left panel: $M_N = 3.5$ GeV, $Y = 5$, $|B_{\ell N}|^2 = 5 \times 10^{-6}$, and $\theta_{LV} = \pi/2$. Right panel: $M_N = 3.5$ GeV, $Y = 5$, $|B_{\ell N}|^2 = 5 \times 10^{-6}$, and $\theta_{LV} = \pi/4$. Solid lines stand for processes including the HNOs effects, while the dashed ones stand for the process with NO-HNOs effects (only amplitude interference effects).

and β_N were calculated taking into account the relative probability of each bin of them, that is, considering the specific contribution of each bin in the final values of $d\Gamma(B_c^\pm)/dL$. Figures 6 and 7 also show the results, including the detector position resolution $\mathrm{Reso}(L) = 1$ mm, for a sample of 50 events simulated from the $d\Gamma(B_c^\pm)/dL$ distributions; this effect is shown by triangles that do not fit perfectly on the continuous curve, which corresponds to the detector with perfect resolution, $\mathrm{Reso}(L) = 0.0$ mm. In addition, the effects of nonfixed γ_N and β_N are manifested by means of a smoothing of the modulation; it can be easily seen by an eyeball comparison between Fig. 5 with Figs. 6 and 7 (left panels).

By comparing left and right panels from Figs. 6 and 7, we can see that the maximum of the difference between the curves runs to the left, i.e., in the right panels the CP violation is maximized when $L \approx 23$ mm, while in the left panels it maximizes at $L \approx 66$ mm. This is mainly due to the fact that the larger M_N implies a shorter lifetime and, consequently, the HN decay in shorter distances.

Figures 8 and 9 show the simulated $dN(B_c^\pm)/dL$ distribution for $M_N = 3.5$, $Y = 5$, $|B_{\ell N}|^2 = 5 \times 10^{-6}$ GeV, and two values of θ_{LV} from a sample of 100 and 1000 events, respectively. We remark that we had simulated the same number of events for processes that involve B_c^+ and its CP conjugate (B_c^-); despite that, from Eq. (6) we know that cross sections of B_c^+ and B_c^- are different if $\theta_{LV} \neq 0$. Both cases include their respective statistical error and consider γ_N and β_N distributed according to the result presented in Fig. 4. From Fig. 8 we can see that there is only a modest difference between $B_c^\pm$ distributions, e.g., in $L = 0$–60 mm, based on what we think, it will not be possible to

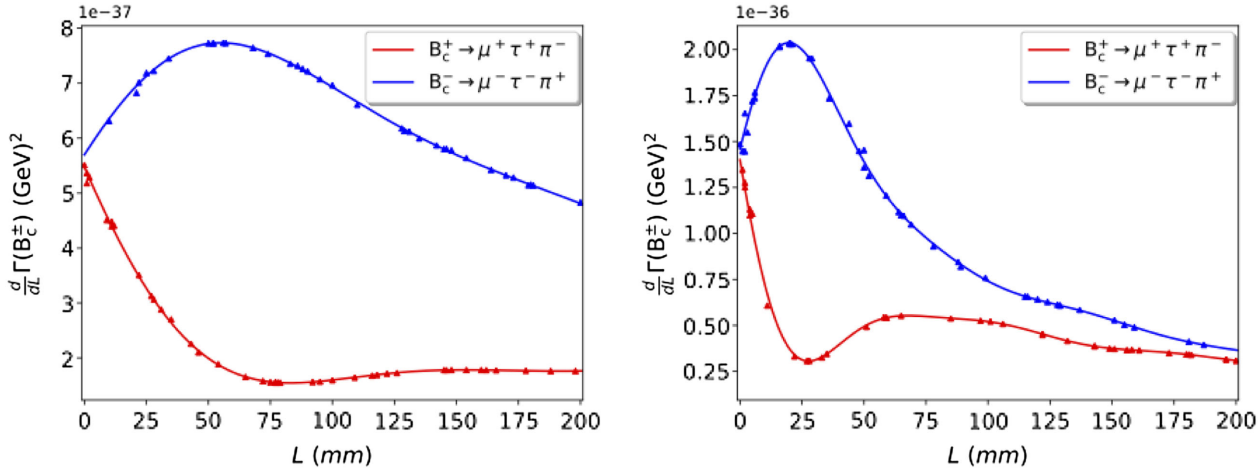

FIG. 6. Differential decay width $d\Gamma(B_c)/dL$ for $\gamma_{B_c^\pm}$ distributed according Fig. 4. Left panel: $M_N = 3.5$ GeV, $Y = 5$, $|B_{\ell N}|^2 = 5 \times 10^{-6}$, and $\theta_{LV} = \pi/2$. Right panel: $M_N = 4.5$ GeV, $Y = 5$, $|B_{\ell N}|^2 = 10^{-5}$, and $\theta_{LV} = \pi/2$. The solid lines are generated assuming perfect detector resolution, while triangles stand for 50 samples of $d\Gamma(B_c)/dL$ convolved with the detector resolution $\mathrm{Reso}(L) = 1.0$ mm.

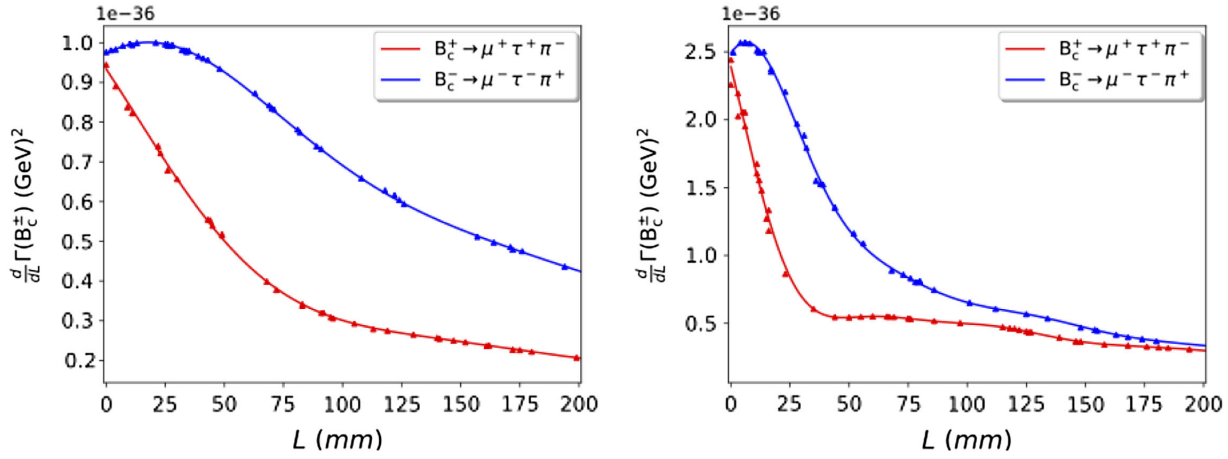

FIG. 7. Differential decay width $d\Gamma(B_c)/dL$ for $\gamma_{B_c^\pm}$ distributed according Fig. 4. Left panel: $M_N = 3.5$ GeV, $Y = 5$, $|B_{\ell N}|^2 = 5 \times 10^{-6}$, and $\theta_{LV} = \pi/4$. Right panel: $M_N = 4.5$ GeV, $Y = 5$, $|B_{\ell N}|^2 = 5 \times 10^{-6}$, and $\theta_{LV} = \pi/4$. The solid lines are generated assuming perfect detector resolution, while triangles stand for 50 samples of $d\Gamma(B_c)/dL$ convolved with the detector resolution Reso$(L) = 1.0$ mm.

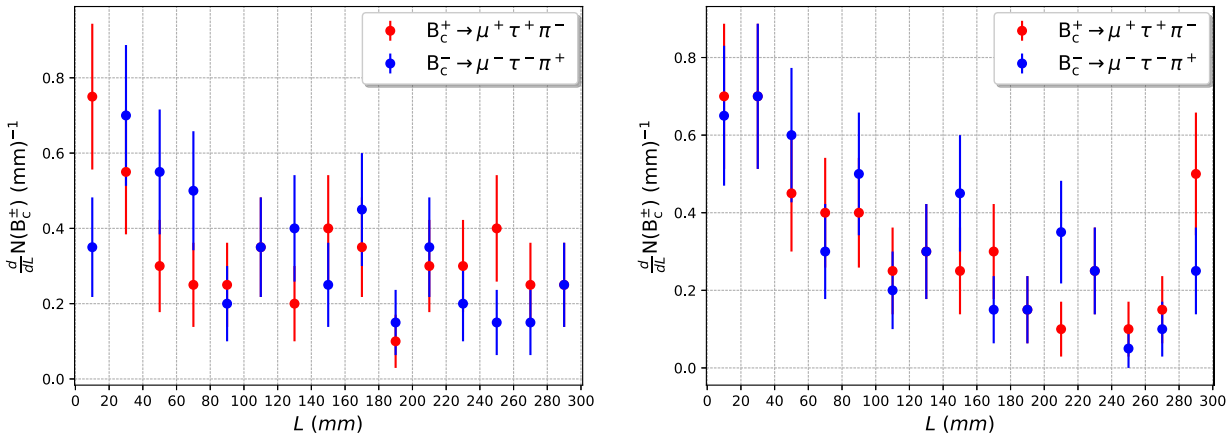

FIG. 8. Differential number of events dN/dL for 100 samples. Left panel: $M_N = 3.5$ GeV, $Y = 5$, $|B_{\ell N}|^2 = 5 \times 10^{-6}$, and $\theta_{LV} = \pi/2$. Right panel: $M_N = 3.5$ GeV, $Y = 5$, $|B_{\ell N}|^2 = 5 \times 10^{-6}$, and $\theta_{LV} = \pi/4$. Here the bin width is $\Delta L = 20$ mm, in addition, it was considered that $\gamma_{B_c^\pm}$ are distributed according Fig. 4.

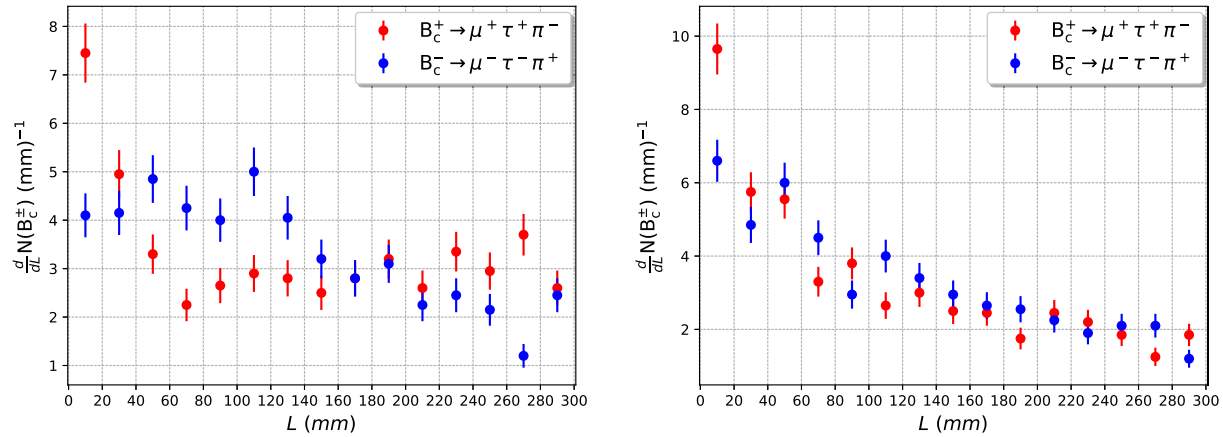

FIG. 9. Differential number of events dN/dL for 1000 samples. Left panel: $M_N = 3.5$ GeV, $Y = 5$, $|B_{\ell N}|^2 = 5 \times 10^{-6}$, and $\theta_{LV} = \pi/2$. Right panel: $M_N = 3.5$ GeV, $Y = 5$, $|B_{\ell N}|^2 = 5 \times 10^{-6}$, and $\theta_{LV} = \pi/4$. Here the bin width is $\Delta L = 20$ mm, in addition, it was considered that $\gamma_{B_c^\pm}$ are distributed according Fig. 4.

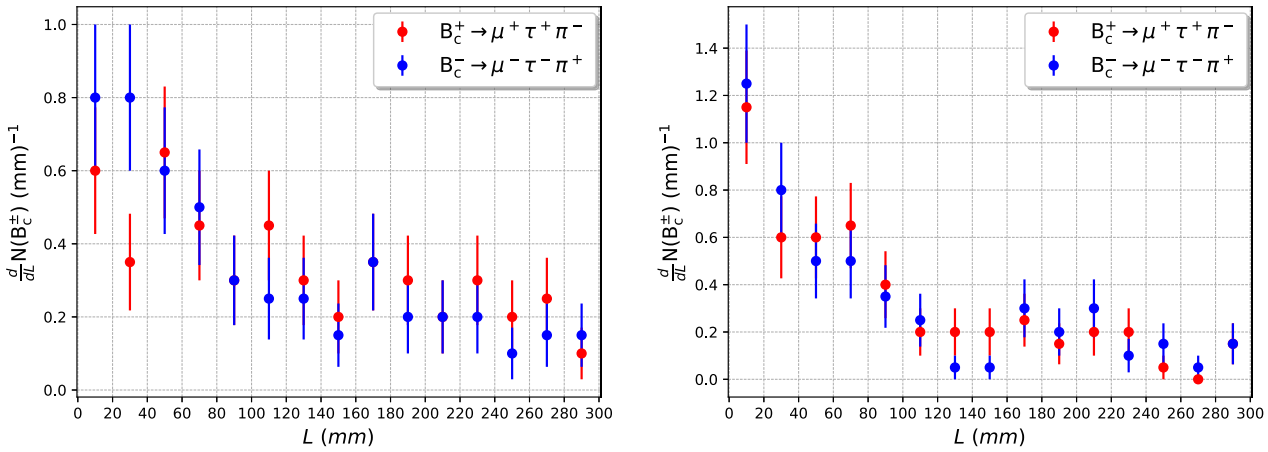

FIG. 10. Differential number of events dN/dL for 100 samples. Left panel: $M_N = 4.5$ GeV, $Y = 5$, $|B_{\ell N}|^2 = 5 \times 10^{-6}$, and $\theta_{LV} = \pi/2$. Right panel: $M_N = 4.5$ GeV, $Y = 5$, $|B_{\ell N}|^2 = 5 \times 10^{-6}$, and $\theta_{LV} = \pi/4$. Here the bin width is $\Delta L = 20$ mm, in addition, it was considered that $\gamma_{B_c^\pm}$ are distributed according Fig. 4.

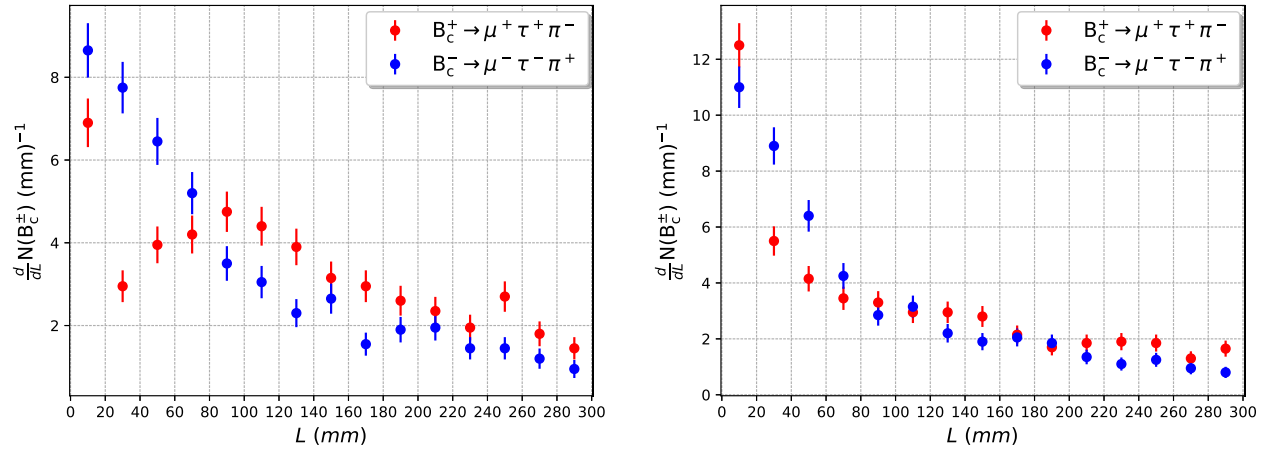

FIG. 11. Differential number of events dN/dL for 1000 samples. Left panel: $M_N = 4.5$ GeV, $Y = 5$, $|B_{\ell N}|^2 = 5 \times 10^{-6}$, and $\theta_{LV} = \pi/2$. Right panel: $M_N = 4.5$ GeV, $Y = 5$, $|B_{\ell N}|^2 = 5 \times 10^{-6}$, and $\theta_{LV} = \pi/4$. Here the bin width is $\Delta L = 20$ mm, in addition, it was considered that $\gamma_{B_c^\pm}$ are distributed according Fig. 4.

distinguish the oscillation for either $\theta_{LV} = \pi/2$ or $\theta_{LV} = \pi/4$ with more than 5σ's from the "nonoscillation" scenario with only 100 signal events. A more positive scenario is shown in Fig. 9, assuming 1000 signal events, where we can clearly observe the oscillation with good precision in the whole range for $\theta_{LV} = \pi/2$ and in $L = 0$–120 mm, $L = 180$–200 mm, and $L = 260$–300 mm for $\theta_{LV} = \pi/4$.

Figures 10 and 11 show the $dN(B_c^\pm)/dL$ distribution for $M_N = 4.5$, $Y = 5$, $|B_{\ell N}|^2 = 5 \times 10^{-6}$ GeV, and two values of θ_{LV} from a sample of 100 and 1000 events, respectively. Both cases include their respective statistical error and consider γ_N and β_N distributed according to the result presented in Fig. 4. For this larger mass scenario, we observed that the feasibility of discovering HN oscillation is possible in the whole range of L for $\theta_{LV} = \pi/2$ and for $L = 20$–60 mm, $L = 140$–160 mm, $L = 220$–260 mm and $L = 280$–300 mm for $\theta_{LV} = \pi/4$, with a similar conclusion about statistics, addressing the 5σ's only in the 1000 signal events case.

V. SUMMARY

In this work we have studied the decay of HNs and their modulation in rare B_c meson decays at the HL-LHCb conditions. Here we have found that the modulation produced by the HNOs could be observed if 1000 HN events are detected; this number is consistent with the expected number of HN decays at HL-LHCb.

ACKNOWLEDGMENTS

The work of J. Z.-S. and M. V.-B. was funded by ANID—Millennium Program—ICN2019_044. The work of S. T. acknowledges support from the U.S. Department of Energy, Office of Science, Nuclear Physics, under Grant No. DE-FG0292ER40962.

[1] Y. Fukuda *et al.* (Super-Kamiokande Collaboration), Phys. Rev. Lett. **81**, 1562 (1998).
[2] K. Eguchi *et al.* (KamLAND Collaboration), Phys. Rev. Lett. **90**, 021802 (2003).
[3] R. N. Mohapatra *et al.*, Rep. Prog. Phys. **70**, 1757 (2007).
[4] R. N. Mohapatra and A. Y. Smirnov, Annu. Rev. Nucl. Part. Sci. **56**, 569 (2006).
[5] S. Weinberg, Phys. Rev. Lett. **43**, 1566 (1979).
[6] J. Zhang, T. Wang, G. Li, Y. Jiang, and G.-L. Wang, Phys. Rev. D **103**, 035015 (2021).
[7] A. Abada, C. Hati, X. Marcano, and A. M. Teixeira, J. High Energy Phys. 09 (2019) 017.
[8] M. Drewes, J. Klarić, and P. Klose, J. High Energy Phys. 11 (2019) 032.
[9] R. M. Godbole, S. P. Maharathy, S. Mandal, M. Mitra, and N. Sinha, Phys. Rev. D **104**, 095009 (2021).
[10] C. Dib, V. Gribanov, S. Kovalenko, and I. Schmidt, Phys. Lett. B **493**, 82 (2000).
[11] G. Cvetic, C. Dib, and C. S. Kim, J. High Energy Phys. 06 (2012) 149.
[12] G. Cvetic, C. Kim, and J. Zamora-Saa, J. Phys. G **41**, 075004 (2014).
[13] G. Cvetic, C. Kim, and J. Zamora-Saa, Phys. Rev. D **89**, 093012 (2014).
[14] G. Cvetic, C. Dib, C. S. Kim, and J. Zamora-Saa, Symmetry **7**, 726 (2015).
[15] G. Cvetic, C. S. Kim, R. Kogerler, and J. Zamora-Saa, Phys. Rev. D **92**, 013015 (2015).
[16] C. O. Dib, M. Campos, and C. Kim, J. High Energy Phys. 02 (2015) 108.
[17] G. Moreno and J. Zamora-Saa, Phys. Rev. D **94**, 093005 (2016).
[18] D. Milanes and N. Quintero, Phys. Rev. D **98**, 096004 (2018).
[19] J. Mejia-Guisao, D. Milanes, N. Quintero, and J. D. Ruiz-Alvarez, Phys. Rev. D **97**, 075018 (2018).
[20] G. Cvetic, C. S. Kim, S. Mendizabal, and J. Zamora-Saa, Eur. Phys. J. C **80**, 1052 (2020).
[21] A. Das, S. Jana, S. Mandal, and S. Nandi, Phys. Rev. D **99**, 055030 (2019).
[22] A. Das and N. Okada, Phys. Lett. B **774**, 32 (2017).
[23] A. Das and N. Okada, Phys. Rev. D **88**, 113001 (2013).
[24] S. Antusch, E. Cazzato, and O. Fischer, Mod. Phys. Lett. A **34**, 1950061 (2019).
[25] A. Das, Y. Gao, and T. Kamon, Eur. Phys. J. C **79**, 424 (2019).
[26] A. Das, P. S. B. Dev, and C. S. Kim, Phys. Rev. D **95**, 115013 (2017).
[27] S. Chakraborty, M. Mitra, and S. Shil, Phys. Rev. D **100**, 015012 (2019).
[28] G. Cvetic and C. S. Kim, Phys. Rev. D **100**, 015014 (2019).
[29] S. Antusch, E. Cazzato, and O. Fischer, Int. J. Mod. Phys. A **32**, 1750078 (2017).
[30] G. Cottin, J. C. Helo, and M. Hirsch, Phys. Rev. D **98**, 035012 (2018).
[31] L. Duarte, G. Zapata, and O. A. Sampayo, Eur. Phys. J. C **79**, 240 (2019).
[32] M. Drewes and J. Hajer, J. High Energy Phys. 02 (2020) 070.
[33] P. S. Bhupal Dev, R. N. Mohapatra, and Y. Zhang, J. High Energy Phys. 11 (2019) 137.
[34] G. Cvetič, A. Das, and J. Zamora-Saá, J. Phys. G **46**, 075002 (2019).
[35] G. Cvetič, A. Das, S. Tapia, and J. Zamora-Saá, J. Phys. G **47**, 015001 (2020).
[36] A. Das, Adv. High Energy Phys. **2018**, 9785318 (2018).
[37] A. Das, P. Konar, and S. Majhi, J. High Energy Phys. 06 (2016) 019.
[38] A. Das, P. S. B. Dev, and R. N. Mohapatra, Phys. Rev. D **97**, 015018 (2018).
[39] D. Milanes, N. Quintero, and C. E. Vera, Phys. Rev. D **93**, 094026 (2016).
[40] J. Zamora-Saa, J. High Energy Phys. 05 (2017) 110.
[41] S. Tapia and J. Zamora-Saá, Nucl. Phys. **B952**, 114936 (2020).
[42] C. S. Kim, G. López Castro, and D. Sahoo, Phys. Rev. D **96**, 075016 (2017).
[43] C. O. Dib, J. C. Helo, M. Nayak, N. A. Neill, A. Soffer, and J. Zamora-Saa, Phys. Rev. D **101**, 093003 (2020).
[44] T. Asaka, S. Blanchet, and M. Shaposhnikov, Phys. Lett. B **631**, 151 (2005).
[45] T. Asaka and M. Shaposhnikov, Phys. Lett. B **620**, 17 (2005).
[46] E. K. Akhmedov, V. A. Rubakov, and A. Y. Smirnov, Phys. Rev. Lett. **81**, 1359 (1998).
[47] R. Aaij *et al.* (LHCb Collaboration), arXiv:2104.04421.
[48] R. Aaij *et al.* (LHCb Collaboration), J. High Energy Phys. 03 (2021) 075.
[49] J.-L. Tastet and I. Timiryasov, J. High Energy Phys. 04 (2020) 005.
[50] A. Atre, T. Han, S. Pascoli, and B. Zhang, J. High Energy Phys. 05 (2009) 030.
[51] J. Alwall, R. Frederix, S. Frixione, V. Hirschi, F. Maltoni, O. Mattelaer, H. S. Shao, T. Stelzer, P. Torrielli, and M. Zaro, J. High Energy Phys. 07 (2014) 079.
[52] T. Sjostrand, S. Mrenna, and P. Z. Skands, Comput. Phys. Commun. **178**, 852 (2008).
[53] J. de Favereau, C. Delaere, P. Demin, A. Giammanco, V. Lemaître, A. Mertens, and M. Selvaggi (DELPHES 3 Collaboration), J. High Energy Phys. 02 (2014) 057.
[54] R. Aaij *et al.* (LHCb Collaboration), arXiv:1808.08865.
[55] R. Aaij *et al.* (LHCb Collaboration), J. High Energy Phys. 12 (2017) 026.
[56] A. V. Berezhnoy, V. V. Kiselev, A. K. Likhoded, and A. I. Onishchenko, Phys. At. Nucl. **60**, 1729 (1997) [arXiv:hep-ph/9703341].